

Investigation of regional seismicity before and after hydraulic fracturing in the Horn River Basin, northeast British Columbia

Amir Mansour Farahbod, Honn Kao, Dan M. Walker, and John F. Cassidy

Abstract: We systematically re-analyzed historical seismograms to verify the existence of background seismicity in the Horn River Basin of northeast British Columbia before the start of regional shale gas development. We also carefully relocated local earthquakes that occurred between December 2006 and December 2011 to delineate their spatiotemporal relationship with hydraulic fracturing (HF) operations in the region. Scattered seismic events were detected in the Horn River Basin throughout the study periods. The located seismicity within 100 km of the Fort Nelson seismic station had a clearly increasing trend, specifically in the Etsho area where most local HF operations were performed. The number of events was increased from 24 in 2002–2003 (prior to HF operations) to 131 in 2011 (peak period of HF operations). In addition, maximum magnitude of the events was shifted from M_L 2.9 to M_L 3.6 as the scale of HF operation expanded from 2006–2007 to 2011. Based on our relocated earthquake catalog, the overall b value is estimated at 1.21, which is higher than the average of tectonic/natural earthquakes of ~ 1.0 . Our observations highly support the likelihood of a physical relationship between HF operation and induced seismicity in the Horn River Basin. Unfortunately, due to the sparse station density in the region, depth resolution is poor for the vast majority of events in our study area. As new seismograph stations are established in northeast British Columbia, both epicentral mislocation and depth uncertainty for future events are expected to improve significantly.

Résumé : Nous analysons à nouveau et de manière systématique des sismogrammes historiques dans le but de vérifier l'existence d'une sismicité de fond dans le bassin de Horn River, nord-est de la Colombie-Britannique, avant le début d'un développement régional de gaz de shale. Nous avons aussi soigneusement relocalisé les séismes locaux survenus entre décembre 2006 et décembre 2011 afin de délimiter leurs relations spatiotemporelles par rapport aux opérations de fracturation hydraulique (FH) dans la région. Des événements sismiques dispersés ont été détectés dans le bassin de Horn River durant toutes les périodes d'étude. La sismicité localisée dans un rayon de 100 km de la station sismique de Fort Nelson montrait nettement une tendance croissante, surtout dans le secteur d'Etsho où se déroulaient la plupart des opérations de FH. Le nombre d'événements a crû de 24 en 2002–2003 (avant les opérations de FH) à 131 en 2011 (période de pointe des opérations de FH). De plus, la magnitude maximale des événements est passée de M_L 2,9 à M_L 3,6 à mesure qu'augmentait l'échelle des opérations de FH de 2006–2007 à 2011. En se basant sur notre catalogue des séismes relocialisés, la valeur b générale est estimée à 1,21, ce qui est supérieur à la moyenne des séismes tectoniques/naturels de $\sim 1,0$. Nos observations supportent fortement la possibilité d'une relation physique entre les opérations de FH et la sismicité induite dans le bassin de Horn River. Malheureusement, en raison de la faible densité des stations dans la région, la résolution de la profondeur est mauvaise pour la plupart des événements dans notre secteur d'étude. À mesure que de nouvelles stations sismiques seront établies dans le nord-est de la Colombie-Britannique, l'erreur de positionnement de l'épicentre et l'incertitude quant à la profondeur des événements futurs devraient diminuer de façon significative. [Traduit par le Rédaction]

Introduction

The Horn River Basin (HRB), located in northeast British Columbia (Fig. 1), is one of the largest shale gas fields in North America (US Department of Energy 2011). As the shale gas exploration and development significantly expanded over the past decade, there have been increasing concerns from governments and local communities on a variety of environmental and public safety issues. Among them, the possibility of increasing seismic hazards due to earthquakes induced by the hydraulic fracturing (HF) treatment of shale gas formations is one of the most discussed topics and has generated serious anxiety in the affected areas (e.g., Green and Styles 2012; Hayes 2012).

It is well known that fluid overpressure would reduce the effective normal stress and thus facilitate shear failures (e.g., Hubbert and Rubey 1959; Pearson 1981). While HF stimulations are very

successful in creating flow channels within shale gas formations, there is growing evidence that high-pressure fluid injection could also induce local earthquakes in areas where historical seismicity is rare (e.g., Horner et al. 1994; Deichmann and Giardini 2009; Frohlich et al. 2011; Holland 2011; Avouac 2012; Frohlich 2012; Ellsworth 2013; Frohlich and Brunt 2013; Maxwell 2013; Keranen et al. 2013, 2014; Schultz et al. 2014). In the HRB, limited HF operations started in late November 2006, became much more active in 2009 as the shale gas development expanded, and increased again in 2010 and 2011 (British Columbia Oil and Gas Commission 2012). In terms of regional seismicity, earthquake catalogues compiled by Natural Resources Canada (NRCan) indicate that the HRB area had only one event before 2009 (15 February 2004, M_L 2.4). Since then, however, more than 40 local earthquakes have been detected and reported (Fig. 2). Among them, seven events in 2010 were determined with $M_L \geq 3$. Such a dramatic change in the pattern of background

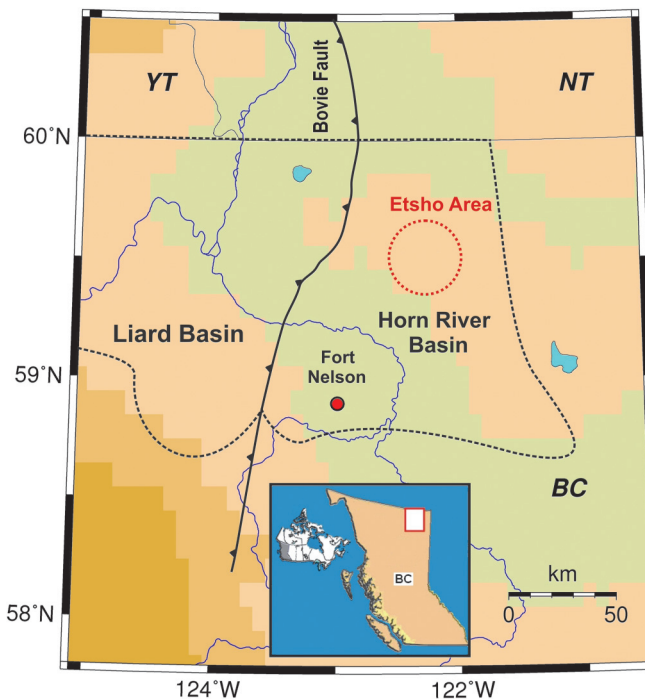
Received 17 September 2014. Accepted 7 December 2014.

Paper handled by Associate Editor Andrew Calvert.

A.M. Farahbod, H. Kao, and J.F. Cassidy. Geological Survey of Canada, Pacific Geoscience Centre, 9860 West Saanich Road, Sidney, BC V8L 4B2, Canada.
D.M. Walker. British Columbia Oil and Gas Commission, 300, 398 Harbour Rd., Victoria, BC V9A 0B7, Canada.

Corresponding author: Amir Mansour Farahbod (e-mail: Amir.Farahbod@NRCan-RNCan.gc.ca).

Fig. 1. A map showing the location of the Horn River Basin and Fort Nelson in northeast British Columbia (BC). The Bovie Fault separates the Horn River Basin from the neighboring Liard Basin. Dashed lines mark the outline of the basin system. YT and NT correspond to Yukon and Northwest Territories, respectively.

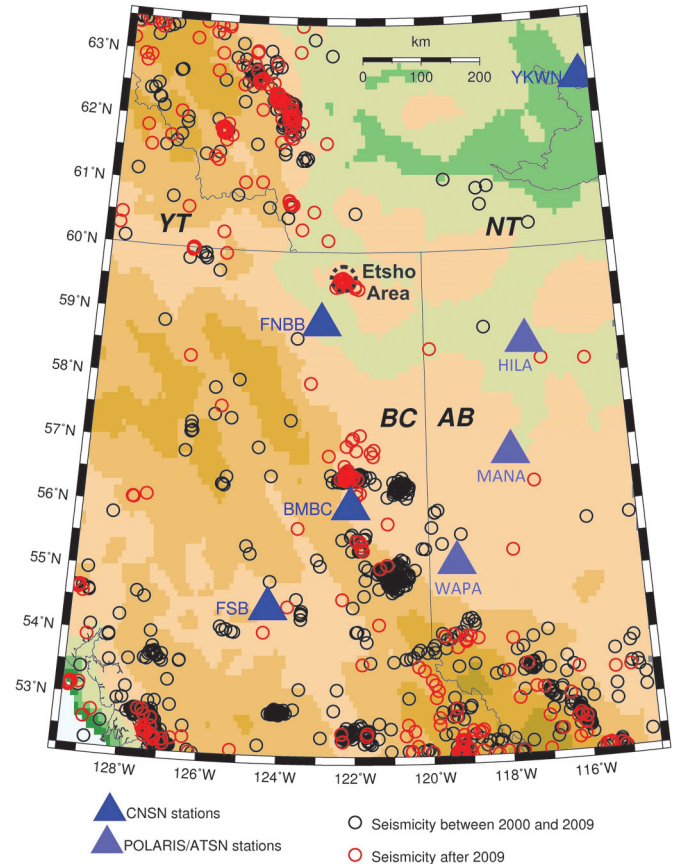


seismicity is unusual. Moreover, areas immediately to the north or west of the HRB, where no shale gas HF was performed, show no discernible variation (Fig. 2).

Delineating possible relationships between local HF operations and the change of seismic pattern in the HRB requires accurate assessment of earthquake distribution both before and after the regional shale gas development. Unfortunately, the Canadian National Seismograph Network (CNSN), which is the primary data source for NRCan's earthquake catalog, had very sparse station coverage for northeast British Columbia before mid-2013. There was only one station in the HRB (at Fort Nelson, FNBB, Fig. 2), and stations to the east, west, and south were all located at least 350 km away. The station distribution was even worse to the north where no seismograph station was available between Yellowknife in the Northwest Territories and Whitehorse in the Yukon. Thus, the apparent lack of historical background seismicity in the HRB could be an artifact due to the poor detection threshold of the CNSN.

To clarify the above issue, we conducted a systematic investigation of the background seismicity for the HRB. Because the conventional earthquake location methods are inapplicable to smaller events whose seismic signals fail to reach multiple stations at distance, we had to take a totally different approach with a very limited dataset. We randomly chose a one-year window (from July 2002 to July 2003) that is well before the start of local HF operations to verify the apparent aseismic nature of the HRB. Also, we applied the same procedure to analyze continuous waveforms from December 2006 until the end of 2011 to better define the spatiotemporal distribution of local seismicity after the beginning of shale gas development in the HRB. These results are then compared to the timing and locations of HF operations in the area, available from the British Columbia Oil and Gas Commission, to investigate their possible relationship.

Fig. 2. Seismicity (circles) between 2000 and mid-2014 and seismograph stations (triangles) in the Horn River Basin and neighboring regions. CNSN, Canadian National Seismograph Network; POLARIS, Portable Observatories for Lithospheric Analysis and Research Investigating Seismicity; ATSN, Alberta Telemetered Seismograph Network.

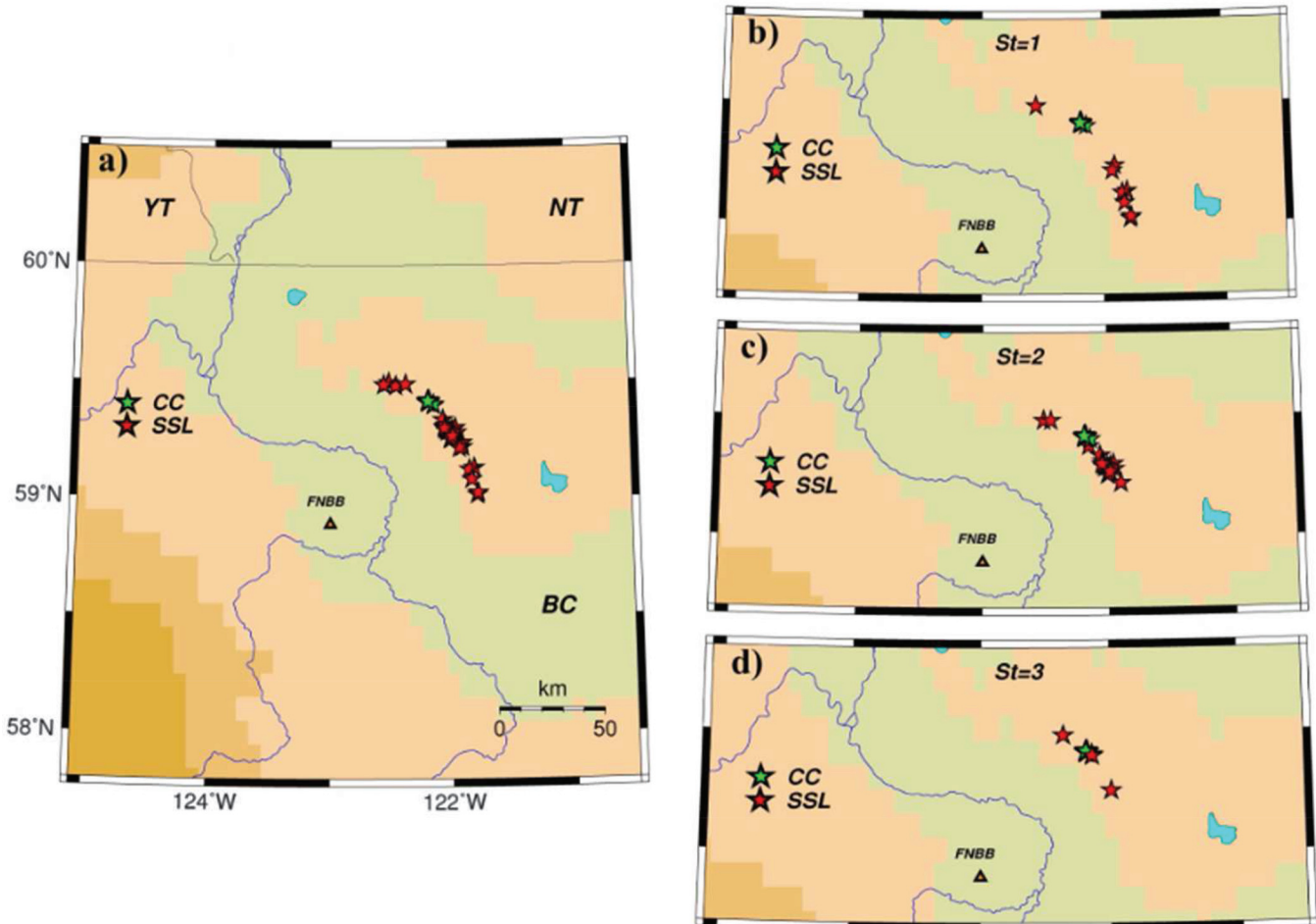


Data and analysis

Our primary dataset is the continuous three-component broadband waveforms from the CNSN station at Fort Nelson (FNBB, Fig. 2). P and S phases were picked by visual inspection of bandpass-filtered (1–5 Hz) seismograms. Whenever corresponding arrivals could be identified, waveforms from other nearby stations in the region (Fig. 2), including Bull Mountain (BMBC), Fort St. James (FSB), Yellowknife (YKWN), and three stations of the Alberta Telemetered Seismograph Network (HILA, MANA, and WAPA), were also included to maximize the constraint.

We use the single-station location (SSL) method to locate hypocenters of local events. Here, we briefly explain how the SSL method works. Readers are referred to the original paper (Roberts et al. 1989) and the user manual for the Seismic Analysis software package (SEISAN, Ottemöller et al. 2012) for more technical details. The principle concept of SSL is to determine the source's hypocenter by tracing back the corresponding ray path. The first step of our analysis is to pick a short time window that contains P arrival on the vertical component seismogram. Cross correlation functions are then calculated respectively between the vertical component and the two horizontal components. The ratio between the two cross correlation functions is used to estimate the back azimuth (i.e., the direction from station to the source). The incident angle is subsequently estimated from the ratio between the cross correlation between the radial and vertical components and the autocorrelation of the vertical component. Finally, the ray path is traced backward from the recording

Fig. 3. Comparison of epicenters determined by the cross-correlation method (CC) and single-station location (SSL) method for local earthquakes in the Horn River Basin. Data from a dense local array are used to derive the CC solutions, whereas SSL solutions use only Canadian National Seismograph Network stations. (a) All 26 events that occurred during July and August of 2011. (b) Small events with $M_L \leq 2.1$. Seismic signals of these events can be identified at only one station. (c) Solutions derived from two stations ($2.1 < M_L < 2.9$). (d) For events larger than $M_L 3.0$, waveforms from three stations can be used in the location process.



station toward the source based on an assumed velocity model, and the hypocenter is located at the point that satisfies the travel time difference between the identified S and P phases.

In case of relatively large events that P and S phases can be identified at more than one station, we measure the S–P time differences from all seismograms, but the back azimuth from only the closest three-component station. This is because back azimuths estimated from distant stations are often unreliable due to their low signal-to-noise ratio (SNR). Including these uncertain estimates would deteriorate the accuracy of our solutions.

The SEISAN software determines how well an incoming P wave is polarized by calculating the correlation coefficient and predicted coherence of three-component waveforms (Roberts et al. 1989; Ottemöller et al. 2012). This parameter can be used to select the optimum solution for back azimuth. For a noise-free linearly polarized signal, the correlation coefficient is equal to 1. In practice, this index should be positive and as high as possible. Results with poor correlation coefficient values are rejected. In such cases, the selected time window that contains the P arrival is shifted slightly in search for the highest correlation coefficient.

Accuracy and uncertainty tests

Before we systematically re-evaluate the pattern of background seismicity of the HRB with the SSL method, we conducted several experiments to carefully assess the accuracy and uncertainty of

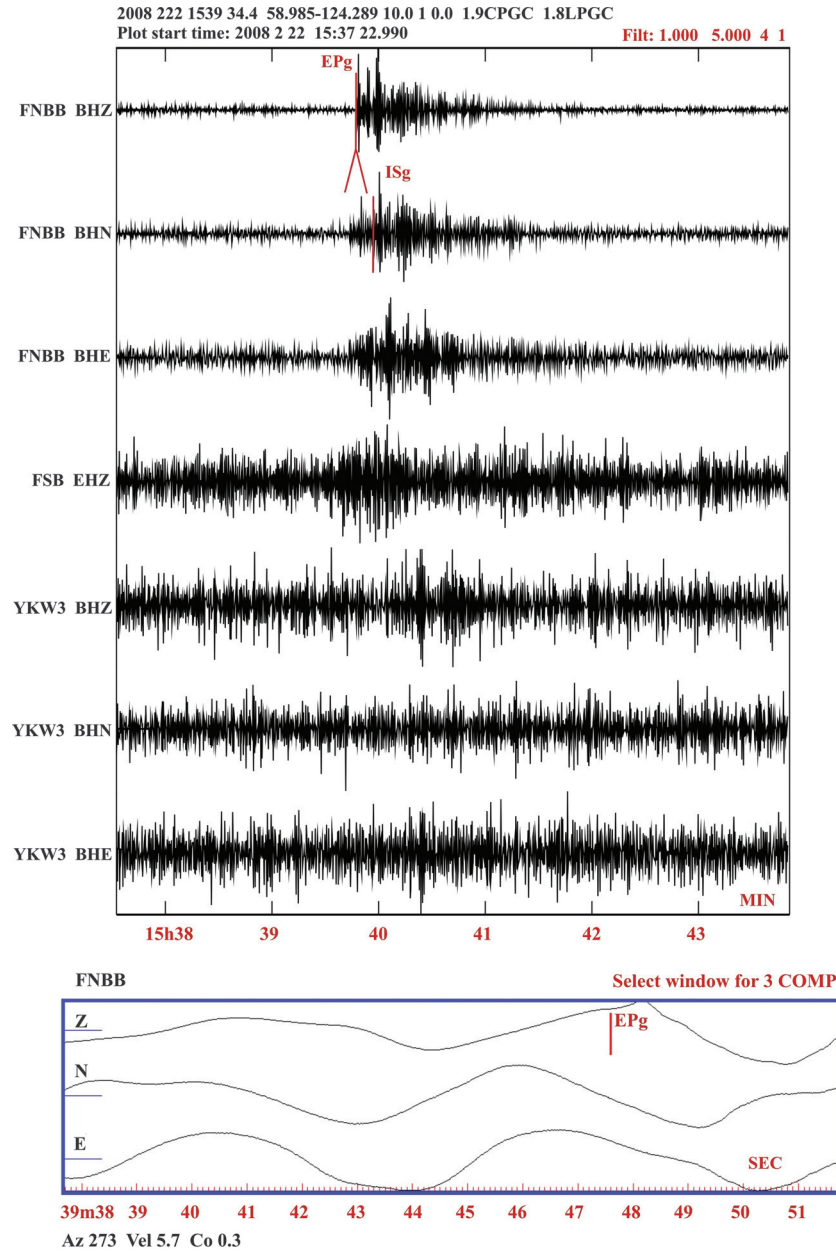
Table 1. Velocity model used in the location process.

Layer	Thickness (km)	V_p (km/s)	V_s (km/s)
1	0.5	5.10	2.95
2	3.5	5.90	3.41
3	5.0	6.20	3.58
4	6.0	6.60	3.81
5	17.0	7.20	4.16
6	4.0	8.20	4.73

the SSL-derived results. Unlike most conventional location methods whose uncertainties are described by an ellipsoid around the best-fitting solution according to the travel time residuals observed at individual stations, the uncertainty of an SSL-derived location is described by two parameters specifying the range of back azimuth and the range of distance. The uncertainty in back azimuth is primarily from the three-component particle motions that define the ray path, whereas the uncertainty in the distance is controlled by the precision of P and S arrival times.

Our first experiment was to use waveform data from station FNBB to locate 26 local events whose hypocenters were well constrained by a temporary dense seismic array deployed during July

Fig. 4. Seismograms corresponding to a small (M_L 1.8) local event that occurred on 22 February 2008. Top panel: Waveforms recorded at the three closest Canadian National Seismograph Network stations. Pg and Sg arrivals can be clearly picked only at station FNBB, while no signals can be recognized at other stations. Bottom panel: A zoom-in window of a few seconds around the picked P first arrival to calculate the corresponding back azimuth (Az), apparent velocity at the surface (Vel), and correlation coefficient (Co).



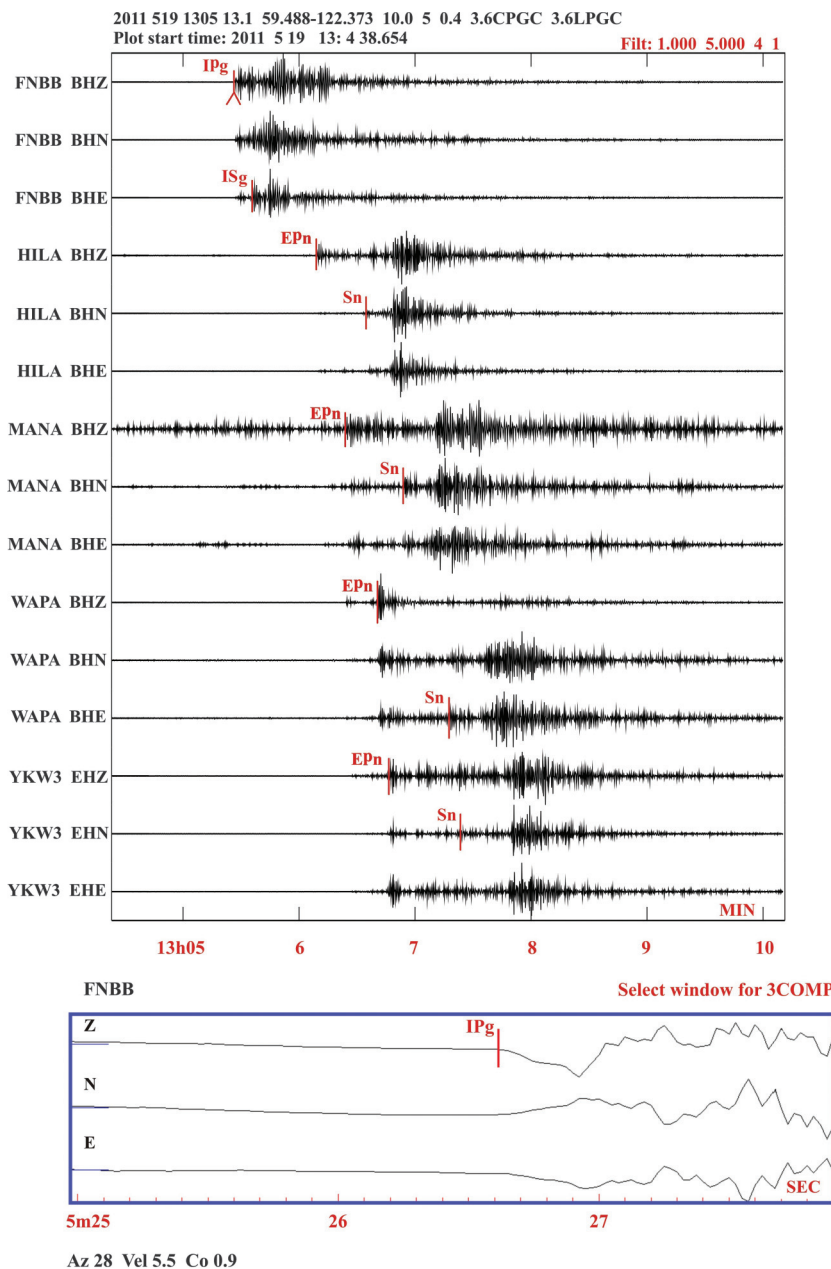
and August of 2011 in one of the HF sites. The size of these local events ranges from M_L 2.0 to 3.1 (British Columbia Oil and Gas Commission 2012). Using only one station, we were able to locate all these events. Taking the locations determined by the local dense array as the ground truth, our results show an error of 0–5 km in distance and from -18° to 39° in back azimuth (Fig. 3a). The means are 2 km and 11.5° , with their standard deviations being 1.4 km and 15° , respectively. If we consider the smallest events ($M_L < 2.2$) that were recorded only by the FNBB station, then the error has a range of 0–3 km in distance and from -18° to 39° in back azimuth (Fig. 3b). The means are 1.5 km and 11.1° , with their standard deviations being 1.5 km and 20.5° , respectively.

Our second experiment was to use waveform data from multiple stations (FNBB, BMBC, YKWN, and FSB) to locate those ground truth events. Due to the sparse distribution of seismograph sta-

tions in the region, we could only conduct this experiment for events with M_L 2.2 or larger. For the 15 events that we could identify their arrivals at two stations, the corresponding distance and back azimuth errors ranged from 0 to 4 km and from -16° to 31° , respectively (Fig. 3c). For the three events that we could identify their arrivals at three stations, the corresponding error in the back azimuth further reduced from -11.6° to 11.5° with a mean of -1.4° (Fig. 3d).

The above experiments show that the location uncertainty is strongly dependent on the number of stations used in the process. Therefore in the worst-case scenario with only one station available, the mislocation error is characterized by a relatively narrow (5 km) arc strip spanning 39° away from the true great-circle path between the epicenter and the station.

Fig. 5. Seismograms corresponding to a local event (M_L 3.6) that occurred on 19 May 2011. Identification of seismic phases can be made at multiple stations (Pg and Sg at FNBB and Pn and Sn at others). Layout and format are the same as that of Fig. 4.



Finally, we repeated the above experiments using a variety of velocity models. Instead of the six-layered velocity model that is used in NRCan's routine determination of earthquake locations (Table 1), we also tried the IASPEI velocity model (Kennett and Engdahl 1991) and a very simple model with one crustal layer over a mantle half-space. With the IASPEI velocity model, our results show an error of 0–6 km in distance and from -17° to 40° in back azimuth. The means are 2 km and 12° , with their standard deviations being 1.7 km and 16° , respectively. These values are statistically equivalent to the results obtained with NRCan's six-layered model, suggesting that the SSL method is tolerant to some velocity model differences. However, the corresponding error in distance increases significantly (up to 11 km) when the oversimplified model consisting of a crustal layer over a mantle half-space is used. The back azimuth error, in contrast, remains almost unchanged (-15° to 38°). This result implies that an incorrect velocity

model probably affects the accuracy of distance much more than that of back azimuth.

Given the same error in back azimuth, the actual epicentral mislocation would increase with distance. To put a cap on the amount of epicentral mislocation due to the back azimuth error and for the practical purpose of monitoring seismicity in the HRB, we only locate earthquakes within 100 km from the station FNBB in this study.

In contrast to the epicenter of a local event, the estimation of focal depth is more challenging. While natural earthquakes in this region can occur in a large depth range, from near the surface to as deep as ~ 35 km, most HF operations are performed along horizontal wells at depths between ~ 2 and 5 km. Therefore, precise determination of focal depth can be a useful factor to discriminate shallow HF-induced earthquakes from deep tectonic events. Unfortunately, the SSL method is not ideal in constraining the

focal depth, especially when the epicentral distance is large. The sparse station coverage in northeast British Columbia before 2013 also made it impossible to obtain a precise depth estimate for regional earthquakes. Therefore, we will not emphasize the focal depth of our results. Each event's waveform characteristics were visually verified, nonetheless, to ensure that they are qualitatively consistent with the derived focal depth (i.e., the existence of strong surface waves means a shallow focal depth, and vice versa). Default depth of 10 km was used for shallow earthquakes in the HRB.

Results

In this section, we first present two representative examples demonstrating the overall quality of our results and how the epicenters are determined from three-component seismograms. Then, we focus on the distribution of background seismicity for three separated time windows: long before the start of HF operations (July 2002–July 2003), during the initial period of light to moderate activity (December 2006–December 2009), and the peak of activity (January 2010–December 2011).

Two representative examples

The first example is a microearthquake whose seismic signals appeared on only one station (Fig. 4). To locate this event, we first picked P and S phase arrivals and assign a quality factor (emergent or impulsive) to each phase depending on the picking time error (top panel, Fig. 4). Then we selected a window of a few seconds around the P wave arrival. At this stage with using all the three components, back azimuth is estimated to be 273°, which corresponds to the highest correlation coefficient value (0.3). Apparent P wave velocity is also determined to be 5.7 km/s (bottom panel, Fig. 4).

The magnitude of this event (M_L) is estimated to be 1.8. Depending on the center frequency of the applied filter (2, 4, 8, and 12 Hz), we calculated the corresponding SNR. This is done by comparing 15 s of noise before the P wave arrival and the last 15 s of S wave coda. The observed SNR value varies between 22 and 40 with an average of 29.7. Given that the observed amplitude is exponentially proportional to the magnitude of the source, such a range of SNR implies that signals from events smaller than 1.0 would be very difficult to be recognized. Therefore it is reasonable to consider 1.0 as the minimum magnitude threshold for this study.

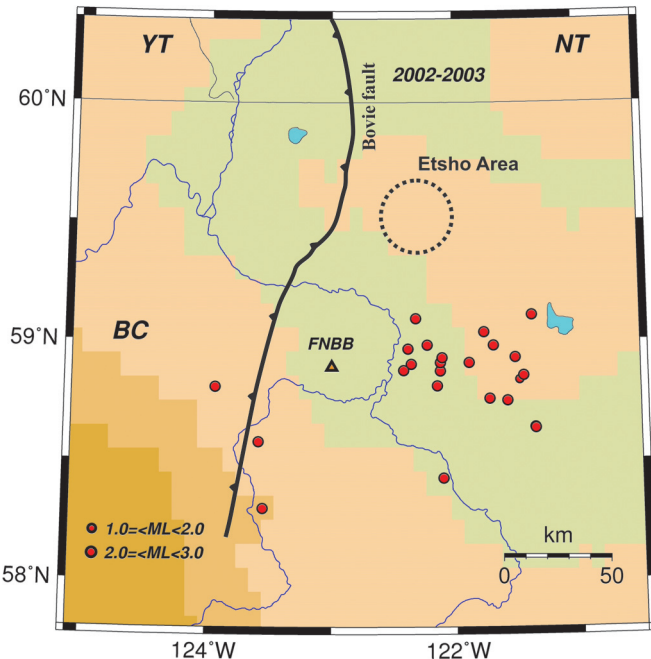
The second event is one of the largest earthquakes ever recorded in the HRB (M_L 3.6). This event was recorded by a number of stations in western Canada and the five closest stations were used in our locating process (Fig. 5). We were able to pick clear P and S phase arrivals at all five stations (Pg and Sg at the closest station FNBB, and Pn and Sn at the others). The back azimuth from FNBB to the source was calculated to be 28° with an excellent correlation coefficient of 0.9. Our final solution indicates that this event occurred 76 km north-northeast from Fort Nelson (59.488°N, 122.373°W). In comparison, the routinely determined epicenter is located at 59.489°N, 122.405°W, which is ~1.8 km from our solution.

Seismicity of the HRB before the start of shale gas production (July 2002 – July 2003)

The NRCan earthquake catalog shows no seismicity in the HRB prior to 2004. To determine whether this lack of background seismicity is a genuine pattern or an artifact due to the sparse seismograph stations in the region, we selected the time window between July 2002 and July 2003 to conduct a systematic SSL analysis in search for any earthquake events that might not be large enough to be detected by CNSN. This time window is more than three years before the start of local HF operations, and thus any detected seismicity must be natural phenomena.

We were able to identify and locate a total of 24 earthquakes with magnitudes ranging from M_L 1.8 to 2.9 (Fig. 6). Most of these

Fig. 6. Background seismicity within 100 km from station FNBB during the period of July 2002 – July 2003. This time window is more than three years before the start of any hydraulic fracturing operations in the Etsho area (dashed circle) of the Horn River Basin. Local earthquakes scattered in the southern part of the Horn River Basin and to the west of FNBB, but no events were detected near Etsho.



events were distributed in the southern HRB to the east of the Bovie fault, which is the major fault system in the region (Maclean and Morrow 2004) separating the HRB and the Liard Basin to the west. It is also interesting to point out that the Etsho area (which is located ~80 km northeast of FNBB, where most of shale gas production wells were drilled later) was apparently aseismic.

The scattered distribution of epicenters confirms the existence of background seismicity in the HRB, but not necessarily at the area of shale gas production. More than 87% of these events were located with data from two or more seismograph stations (Table 2). According to our accuracy and uncertainty test results, their corresponding range of mislocation is 0–4 km in epicentral distance and from -16° to 31° in back azimuth. Such a location precision is considered reasonable for regional seismicity.

Seismicity of the HRB during the initial period of HF operation (December 2006 – December 2009)

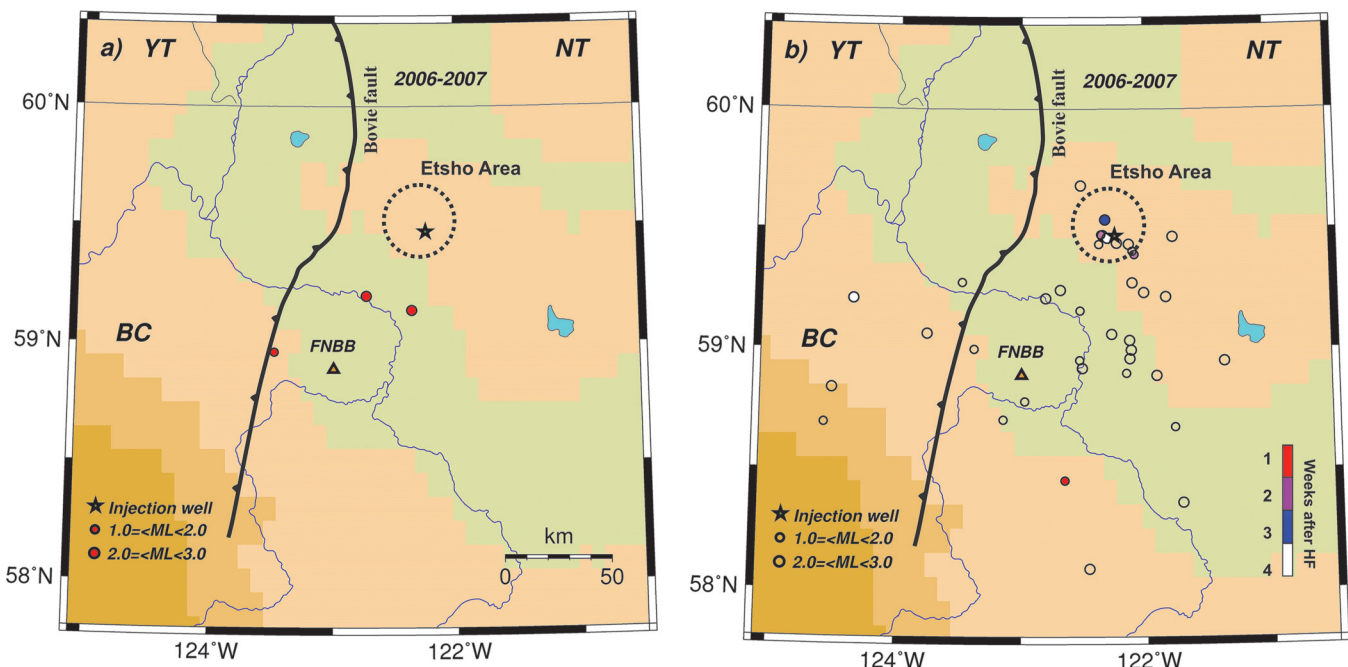
Very limited HF operations were started in the Etsho area of the HRB during the final days of November 2006. There was no trace of visible seismic activity at the FNBB station in November, but we were able to locate three local events in December 2006. HF operations resumed in 2007 for several days near the end of February and another two weeks in March. For the entire 2007, a total of 39 events were located with M_L in the range of 1.3–2.9. Three of these earthquakes occurred during the days of HF operations, but there is no spatial correlation between them and the location of HF fluid injection wells (Fig. 7).

In contrast, we located more events in 2008 (63 events) and 2009 (44 events) as the number of HF days gradually increased (Table 2). The magnitude range, however, appeared to stay effectively unchanged: between M_L 1.0 and 3.0 for events in 2008 (Fig. 8) and between M_L 1.4 and 3.1 for events in 2009 (Fig. 9). It is important to point out that more activity was observed close to injection wells

Table 2. Percentage of days per year when hydraulic fracturing (HF) operation was performed and detected local seismic events in the Horn River Basin.

Year	HF days per year (%)	Total no. of events	Total no. of events during HF	Solutions from one station (%)	Solutions from two stations (%)	Solutions from three stations or more (%)
2002–2003	0	24	0	12.5	62.5	25.0
2006	1.9	3	0	0	100	0
2007	6.8	39	3	56.4	38.5	5.1
2008	14.2	63	33	55.5	41.3	3.2
2009	15.0	44	32	29.6	56.8	13.6
2010	82.5	58	54	19.0	48.3	32.7
2011	84.9	131	119	10.7	50.4	38.9

Fig. 7. Seismicity within 100 km of station FNBB during the initial stage of shale gas development in the Horn River Basin (December 2006–December 2007; ~7% hydraulic fracturing (HF) days per year). Stars mark the locations of HF injection wells. (a) Events that occurred during the times of local HF operation. (b) Events that occurred during non-HF days. Epicenters are marked as solid or open circles if the time lapse between the end of previous HF operation and the origin time is within or greater than one month, respectively.



during the days of HF operations rather than in between the intervals. This is while the number of HF operation days is just a fraction (between 1.9% and 15%) of the year (Table 2). Furthermore, events that occurred during non-HF days tend to cluster around the Etsho area (Figs. 7b and 8b). Many of them happened shortly after the end of HF operation (often within a couple of weeks, Figs. 7b and 8b). The observed spatiotemporal pattern of local seismicity is unlikely to be artifacts due to epicenter mislocation because most events were located using data from two or more stations (Table 2).

Based on the spatiotemporal distribution of the observed seismicity, it is highly likely that local HF operation in 2008 and 2009 might have disturbed the regional stress regime, which in turn resulted in some seismic events. In other words, the observed seismicity can be interpreted as fault movement in response to local variations of stress due to sudden increase of fluid volume associated with HF injection. Within the HRB, the shallow, very high permeability Mississippian Debolt zone is being used for water disposal. Therefore the possibility of induced seismicity due to waste water disposal is considered to be very low (Jeff Johnson, personal communications).

Seismicity of the HRB during the peak period of HF operation (January 2010 – December 2011)

The years of 2010 and 2011 correspond to the peak period of local HF operations. Not only was there a sharp increase in the total volume of injected fluids (5 to 10 times), but also the time windows of HF operation were significantly longer (Table 2). There were more than 300 HF days in each year in 2010 and 2011, which are in great contrast to that during 2006–2009.

We located 58 events in 2010 (Figs. 10a and 10b) and 131 earthquakes in 2011 (Figs. 10c and 10d). The observed magnitude range also clearly shifted to higher values: M_L between 1.6 and 3.6 in 2010–2011. Spatially, the concentration of observed earthquakes near the injection wells during HF operations in this two-year time period is more obvious than ever (Fig. 10). But due to mislocation errors, general trend of the located earthquakes in the Etsho area resembles an arch (Fig. 10c). Temporally, the occurrence of earthquakes during non-HF days is significantly fewer than HF days. However, this is probably biased due to the fact that HF operation was performed during the majority of the days in 2010 and 2011 (Table 2).

Due to the generally larger magnitudes of observed events, we were able to locate approximately one third of events (32.7% for

Fig. 8. Seismicity within 100 km of station FNBB during the year of 2008. Layout and format are the same as that in Fig. 7 ($\sim 14\%$ hydraulic fracturing (HF) days per year).

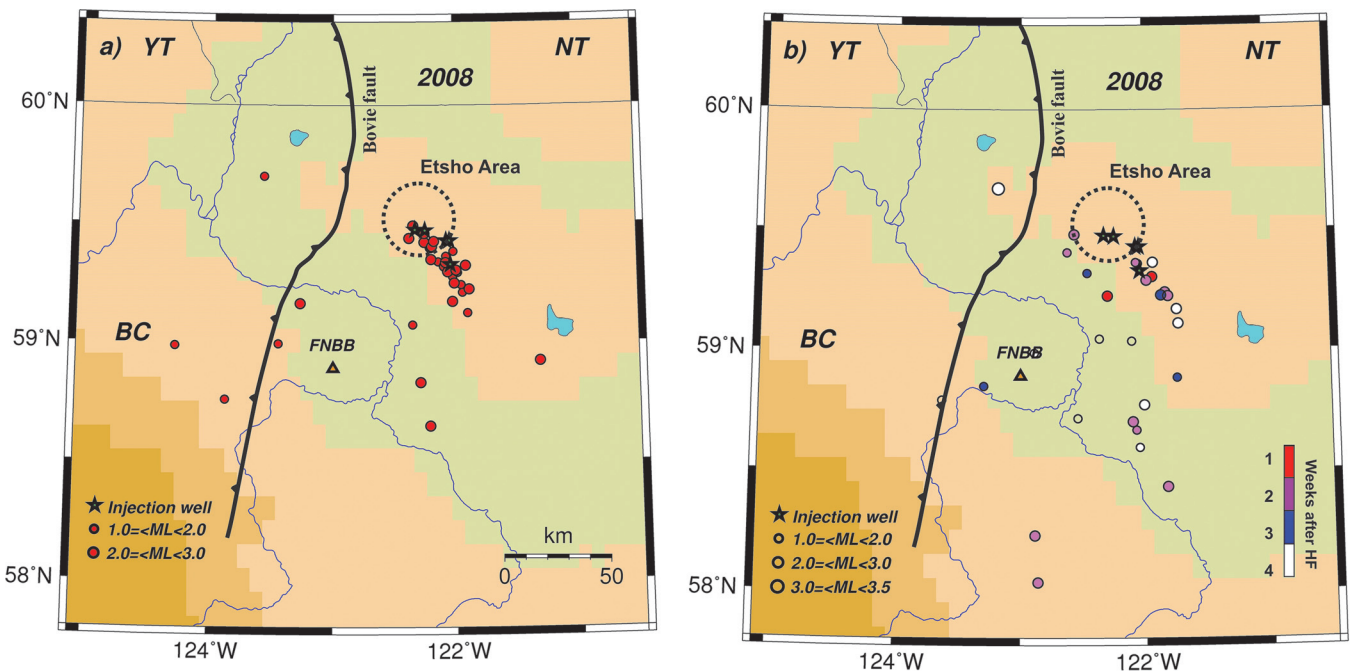
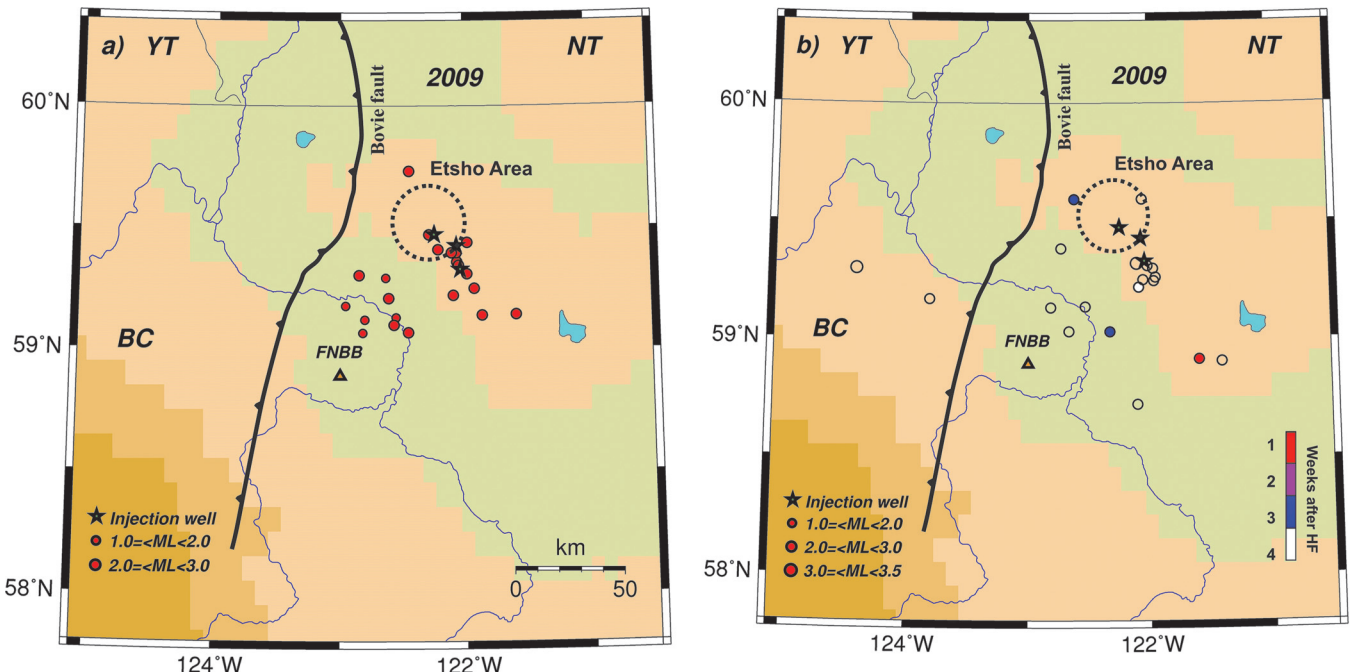


Fig. 9. Seismicity within 100 km of station FNBB during the year of 2009. Layout and format are the same as that in Fig. 7 ($\sim 15\%$ hydraulic fracturing (HF) days per year).



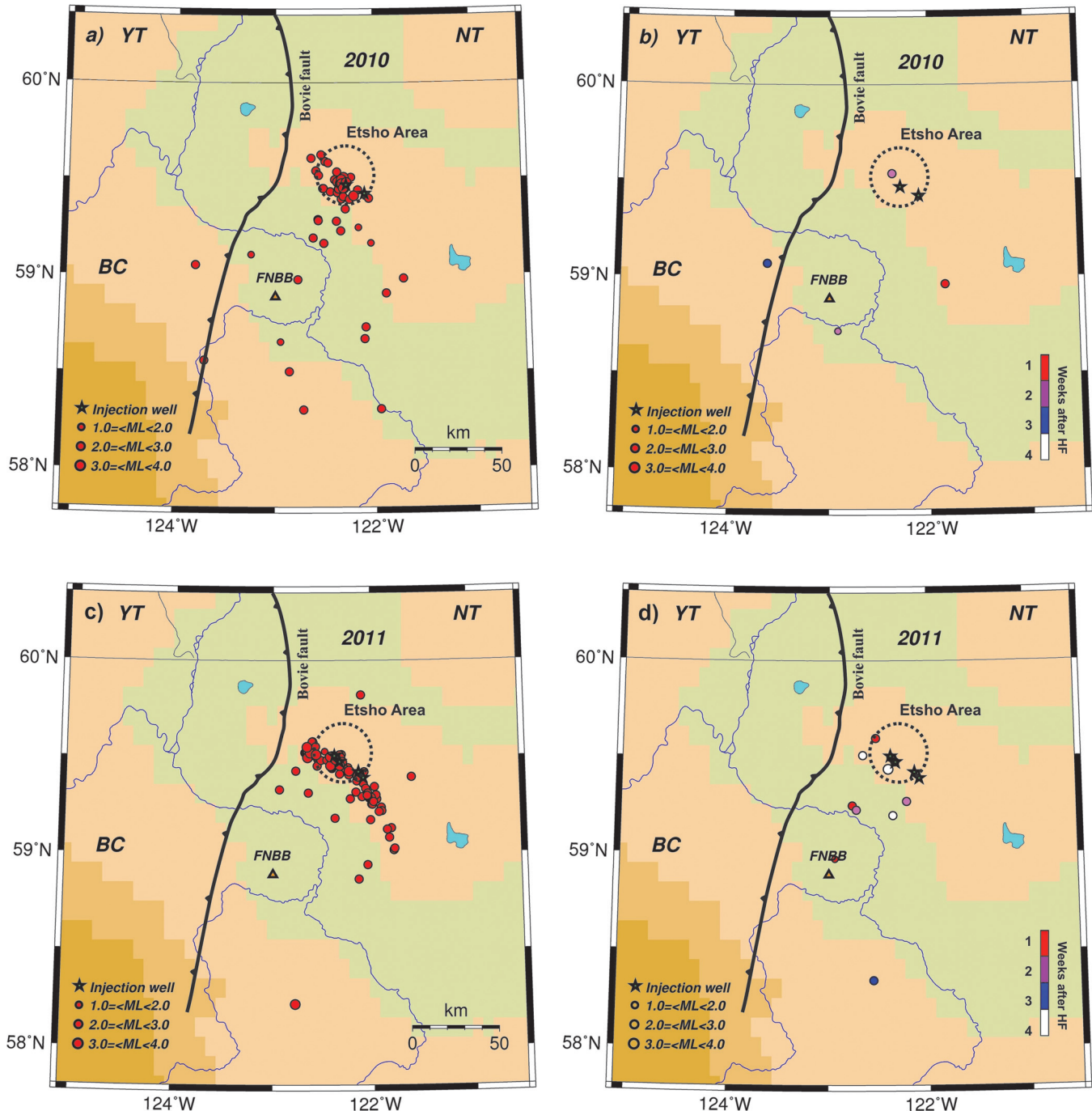
2010 and 38.9% for 2011) with arrival times from three stations or more. With the vast majority of events being better constrained by multiple stations, this time period is expected to have the greatest location precision.

Discussion and conclusions

It is important to point out that establishing positive correlation between earthquake source locations and HF operations in both time and space is only a necessary condition to infer the link

between the two phenomena. Our re-analysis of historical seismograms confirms the existence of background seismicity in the HRB (in 2002–2003) before the start of HF. Scattered seismic events were detected in the region throughout the study periods of 2002–2003 and 2006–2011. Within 100 km of the FNBB station and specifically in the Etsho area where most local HF operations were performed, we observe an increasing trend of earthquake activities in both quantity and magnitude. The number of events was increased from 24 in 2002–2003 to 131 in 2011, and the maximum

Fig. 10. Seismicity within 100 km of station FNBB during (a) and (b) the year of 2010 (~82% hydraulic fracturing (HF) days per year), and (c) and (d) the year of 2011 (~85% HF days per year). Layout and format are the same as that in Fig. 7. Notice that the spatiotemporal distribution of local seismicity in this period appears to highly correlate with the local HF operations. Moreover, both the number and the maximum size of seismic events have increased with respect to those of previous years.



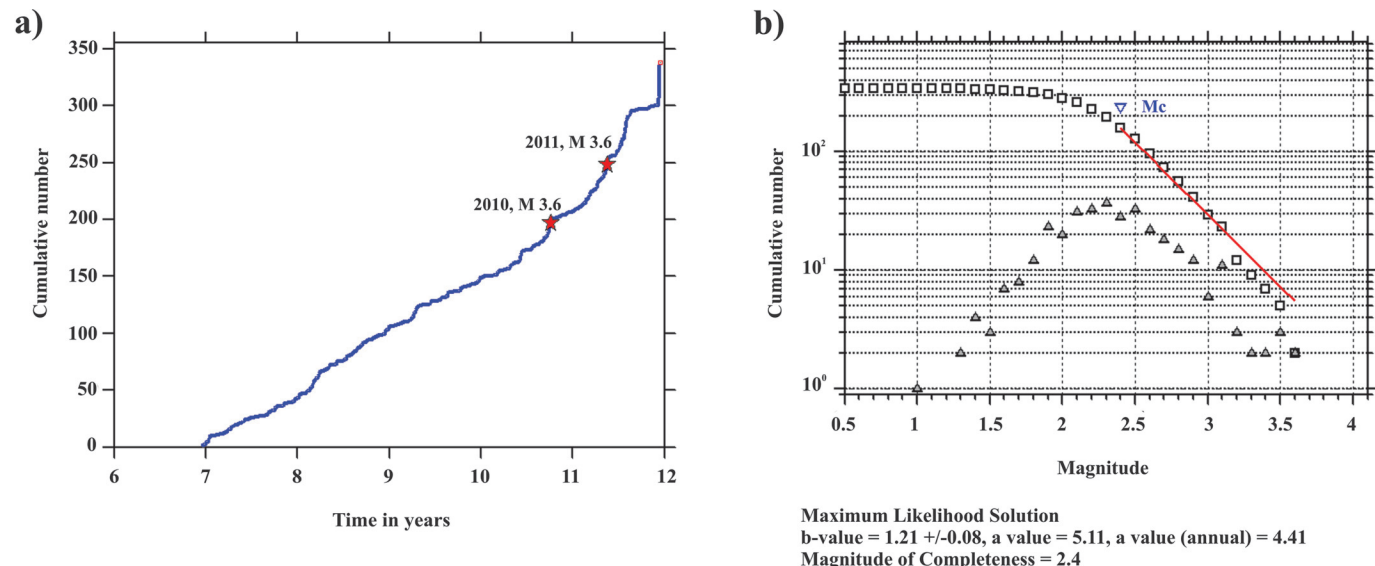
observed magnitude of earthquakes was shifted from M_L 2.9 in 2006–2007 to M_L 3.6 in 2010–2011 as the scale of HF operation expanded over the years.

The correlation between the increasing number of local earthquakes and HF operations can be further demonstrated by the change of average earthquake occurrence rate. For the year of 2002–2003 when all earthquakes were considered natural, the average earthquake occurrence rate is ~2 events per month. Such a rate is very close to the rates derived from the numbers of earthquakes during non-HF days in the first few years (between ~1

and ~3 for 2007–2009, Table 2). In contrast, the number of local earthquakes per month during HF days jumps by almost an order (between ~4 and ~19) for the same time period. In 2011 when the HF operation reached its peak, not only the monthly occurrence rate during HF days increased by a factor of ~6 but also the rate during non-HF days jumped more than three times as well. The dramatic variation in earthquake occurrence rate seems to suggest a link to local HF operations.

Furthermore, if we compare the local earthquake patterns inside and outside of the Etsho area, the difference between HF and

Fig. 11. (a) Cumulative number of located earthquakes as a function of time and (b) relationship between number and magnitude of local earthquakes in the Horn River Basin based on the catalog determined in this study. Triangles mark the numbers of events per individual magnitude bins, whereas squares correspond to the cumulative number of events. The corresponding b value (i.e., the negative slope of the line) is 1.21 with an estimated magnitude of completeness (M_c) of 2.4. All parameters are listed at the bottom.



non-HF days is even more evident. For the area outside of Etsho, the observed seismic pattern appears to be similar to that of 2002–2003 without any temporal trend (i.e., local events scattered in the region; Figs. 7–10). For the Etsho area, however, the concentration of local earthquakes during HF days is remarkably higher compared to non-HF days. This is another hint to suggest that local HF operations can induce more local earthquakes.

It has been demonstrated that the relationship between the number of earthquakes and their size is different for various types of earthquakes depending on their natures (Wessels et al. 2011). For reactivated tectonic microseismic events, the logarithm of the number of events is negatively proportional to the value of magnitude, resulting in a b value around 1. In contrast, the b value is significantly higher (~2) for microseismicity associated with HF injection.

In the HRB, b value analysis of 70 000 microearthquakes (magnitude ranging from –1.7 to 0.5) recorded by a dense seismograph network at one HF site and 135 events (magnitude ranging from 0.6 to 3.2) suggested that smaller local events might be more consistent with fracture-driven mechanisms and larger ones are probably associated with shear dislocation along fault planes (British Columbia Oil and Gas Commission 2012). The magnitude range of our earthquake catalog is clearly higher than the result derived from local array data due to larger distance between earthquake source and recording stations. Based on the entire 338 events that we have located (Fig. 11a), we analyzed the earthquake frequency-magnitude relationship using the maximum likelihood method (e.g., Aki 1965; Wiemer and Wyss 1997; Goertz-Allmann and Wiemer 2013), and the overall b value is estimated at 1.21 (Fig. 11b). The corresponding completeness of our catalog is M_c 2.4. Our derived b value is higher than the average of tectonic/natural earthquakes, but lower than the value of typical HF-induced events, perhaps also implying that at least some of the observed events are related to local HF operation.

Precise determination of earthquake focal depths could also be a key in distinguishing induced seismicity from tectonic/natural earthquakes. In general, source depth is much more difficult to constrain than epicentral location because the travel time residuals become less sensitive to depth variation once the source-station distance is significantly greater than source depth. Unfortunately, this was exactly the scenario for the vast majority of events in our

catalog due to the sparse station density in the region. As new seismograph stations are established in northeast British Columbia, both epicentral mislocation and depth uncertainty for future events are expected to improve significantly.

It would be most useful if we can establish a quantitative model to predict the geo-mechanical response of a shale gas system after HF treatment. Such a model will require detailed knowledge of subsurface structures and sophisticated theoretical development and (or) enormous numerical computation power. At this stage, we are focusing on the establishment of observational foundations. Our results could be valuable in the future in the calibration of configuration parameters as theoretical models are developed.

Finally, application of new processing algorithms to improve earthquake depth resolution with sparse data will help to unambiguously prove the inferred relationship.

Acknowledgements

The Canadian National Seismograph Network and its data management centre are operated and maintained by the Canadian Hazard Information Service. We benefited from discussions with Jeff Johnson, Denis Lavoie, Gail Atkinson, Jason Hendrick, and Virginia Stern. Also, we gratefully acknowledge Gail Atkinson and an anonymous reviewer for their thorough reviews of this manuscript and BCOGC for providing HF data. We used GMT for plotting maps, ZMAP for b value estimation, and Seisan for earthquake locating process. This research is partially supported by a grant from the ecoENERGY Innovation Initiative and a grant from the Natural Sciences and Engineering Research Council of Canada (NSERC) to H.K. This paper is Earth Sciences Sector (ESS) contribution number 20140240.

References

- Aki, K. 1965. Maximum likelihood estimate of b in the formula $\log N = a - bM$ and its confidence limits. Bulletin of Earthquake Research Institute of Tokyo University, 43(2): 237–239.
- Avouac, J.P. 2012. Earthquakes: human-induced shaking. Nature Geoscience, 5: 763–764. doi:10.1038/ngeo1609.
- British Columbia Oil and Gas Commission. 2012. Investigation of observed seismicity in the Horn River Basin. BCOGC Report. Available from www.bcofc.ca/node/8046/download?documentID=1270.
- Deichmann, N., and Giardini, D. 2009. Earthquakes induced by the stimulation of an enhanced geothermal system below Basel (Switzerland). Seismological Research Letters, 80(5): 784–798. doi:10.1785/gssrl.80.5.784.

- Ellsworth, W.L. 2013. Injection-induced earthquakes. *Science*, **341**(6142). doi:[10.1126/science.1225942](https://doi.org/10.1126/science.1225942).
- Frohlich, C. 2012. Two-year survey comparing earthquake activity and injection-well locations in the Barnett Shale, Texas. *Proceedings of the National Academy of Sciences*, **109**: 13934–13938. doi:[10.1073/pnas.1207728109](https://doi.org/10.1073/pnas.1207728109).
- Frohlich, C., and Brunt, M. 2013. Two-year survey of earthquakes and injection-production wells in the Eagle Ford Shale, Texas, prior to the M_W 4.8 20 October 2011 earthquake. *Earth and Planetary Science Letters*, **379**(1): 56–63. doi:[10.1016/j.epsl.2013.07.025](https://doi.org/10.1016/j.epsl.2013.07.025).
- Frohlich, C., Hayward, C., Stump, B., and Potter, E. 2011. The Dallas-Fort Worth earthquake sequence: October 2008 through May 2009. *Bulletin of the Seismological Society of America*, **101**: 327–340. doi:[10.1785/0120100131](https://doi.org/10.1785/0120100131).
- Goertz-Allmann, B.P., and Wiemer, S. 2013. Geomechanical modeling of induced seismicity source parameters and implications for seismic hazard assessment. *Geophysics*, **78**: KS25–KS39. doi:[10.1190/geo2012-0102.1](https://doi.org/10.1190/geo2012-0102.1).
- Green, C.A., and Styles, P. 2012. Preese Hall shale gas fracturing: review and recommendations for induced seismicity mitigation. Available from https://www.gov.uk/government/uploads/system/uploads/attachment_data/file/48330/5055-preese-hall-shale-gas-fracturing-review-and-recomm.pdf.
- Hayes, D.J. 2012. Is the recent increase in felt earthquakes in the central US natural or manmade? U.S. Department of the Interior. Available from <http://www.doi.gov/news/doinews/Is-the-Recent-Increase-in-Felt-Earthquakes-in-the-Central-US-Natural-or-Manmade.cfm>.
- Holland, A. 2011. Examination of possibly induced seismicity from hydraulic fracturing in the Eola Field, Garvin County, Oklahoma. *Oklahoma Geological Survey, Open File Report OF1-2011*. 31 p.
- Horner, R.B., Barclay, J.E., and MacRae, J.M. 1994. Earthquakes and hydrocarbon production in the Fort St. John area of northeastern British Columbia. *Canadian Journal of Exploration Geophysics*, **30**(1): 39–50.
- Hubbert, M.K., and Rubey, W.W. 1959. Role of fluid pressure in mechanics of overthrust faulting. *Geological Society of America Bulletin*, **70**: 115–206. doi:[10.1130/0016-7606\(1959\)70\[115:ROFPM\]2.0.CO;2](https://doi.org/10.1130/0016-7606(1959)70[115:ROFPM]2.0.CO;2).
- Kennett, B.L.N., and Engdahl, E.R. 1991. Travel times for global earthquake location and phase identification. *Geophysical Journal International*, **105**(2): 429–465. doi:[10.1111/j.1365-246X.1991.tb06724.x](https://doi.org/10.1111/j.1365-246X.1991.tb06724.x).
- Keranen, K.M., Savage, H.M., Abers, G.A., and Cochran, S. 2013. Potentially induced earthquakes in Oklahoma, USA: links between wastewater injection and the 2011 M_W 5.7 earthquake sequence. *Geology*, **41**(6): 699–702. doi:[10.1130/G34045.1](https://doi.org/10.1130/G34045.1).
- Keranen, K.M., Weingarten, M., Abers, G.A., Bekins, B.A., and Ge, S. 2014. Sharp increase in central Oklahoma seismicity since 2008 induced by massive wastewater injection. *Science*, **345**(6195): 448–451. doi:[10.1126/science.1255802](https://doi.org/10.1126/science.1255802). PMID: 24993347.
- MacLean, B.C., and Morrow, D.W. 2004. Bovie structure: its evolution and regional context. *Bulletin of Canadian Petroleum Geology*, **52**(4): 302–324. doi:[10.2113/52.4.302](https://doi.org/10.2113/52.4.302).
- Maxwell, S. 2013. Unintentional seismicity induced by hydraulic fracturing. *Canadian Society of Exploration Geophysics Recorder*, **38**(8): 40–49.
- Ottomöller, L., Voss, P., and Havskov, J. 2012. SEISAN earthquake analysis software. [computer program]. University of Bergen, Bergen, Norway.
- Pearson, C. 1981. The relationship between microseismicity and high pore pressures during hydraulic stimulation experiments in low permeability granitic rocks. *Journal of Geophysical Research: Solid Earth*, **86**(B9): 7855–7864. doi:[10.1029/JB086iB09p07855](https://doi.org/10.1029/JB086iB09p07855).
- Roberts, R.G., Christoffersson, A., and Cassidy, F. 1989. Real-time event detection, phase identification and source location estimation using single station three-component seismic data. *Geophysical Journal International*, **97**: 471–480. doi:[10.1111/j.1365-246X.1989.tb00517.x](https://doi.org/10.1111/j.1365-246X.1989.tb00517.x).
- Schultz, R., Stern, V., and Gu, Y.J. 2014. An investigation of seismicity clustered near the Cordel Field, west central Alberta, and its relation to a nearby disposal well. *Journal of Geophysical Research: Solid Earth*, **119**: 3410–3423. doi:[10.1002/2013JB010836](https://doi.org/10.1002/2013JB010836).
- U.S. Department of Energy. 2011. World shale gas resources: an initial assessment of 14 regions outside the United States. U.S. Energy Information Administration Report. Available from http://www.marcellus.psu.edu/resources/PDFs/WorldShaleGas_USEIA.pdf.
- Wessels, S.A., Dela Pena, A., Kratz, M., Williams-Stroud, S., and Jbeili, T. 2011. Identifying faults and fractures in unconventional reservoirs through microseismic monitoring. *First Break*, **29**(7): 99–104.
- Wiemer, S., and Wyss, M. 1997. Mapping the frequency-magnitude distribution in asperities: an improved technique to calculate recurrence times? *Journal of Geophysical Research*, **102**(B7): 15115–15128. doi:[10.1029/97JB00726](https://doi.org/10.1029/97JB00726).